

Article

The Dynamic Behavior of a Single Semiflexible Ring Chain in a Linear Polymer Matrix

Xiaolin Zhou *  and Yifan Qin

College of Physics and Optoelectronic Engineering, Harbin Engineering University, Harbin 150001, China; q1025hb007@163.com

* Correspondence: xlzhou@hrbeu.edu.cn

Abstract: We studied the dynamic behavior of a single semiflexible ring in linear chain matrix based on a coarse-grained model using the molecular dynamics simulation approach. We found that that ring chains' hollow centers are frequently filled with linear chains. However, as the rigidity of the linear chains increases, the linear chains arranged parallel to each other and the ring chain are temporary caged. As a result, the swing movement in the normal direction of the ring is significantly limited, and the relaxation time in the normal direction increases significantly. Our findings can help to understand the physical mechanism of the movement of the ring chain in ring-linear polymer blends at the microscopic level.

Keywords: molecular dynamic simulation; ring-linear blends; semiflexible ring polymer; diffusion

1. Introduction

Ring polymers have no chain end groups and a cyclic structure. They have specific characteristics because of their topology, including a small hydrodynamic volume, a slower rate of deterioration, improved stability, and a higher glass transition temperature [1–10]. Ring polymer chains are present in biosystems [11–18] and have applications in biomedicine [19]. Ring macromolecules gained popularity after Jacob and Wollman found that the genetic map of *E. coli* chromosomes was circular [20]. The biological features of cyclic polymers in vivo are extremely valuable [21]. It was discovered that the cyclic structure allows for a longer circulation period in the bloodstream, as well as a different biodistribution profile when compared to linear polymers of the same molecular weight [21]. Polymer scientists predict a wide range of application prospects for ring polymers based on this distinct feature, particularly for applications in biomedicine (such as drug delivery) [21], microelectronics (such as micro- and nanolithography) [22], and wastewater treatment [23]. In the method of micelle-based drug administration, for instance, the cyclic block copolymer may be formed into micelles with a small size and high stability, which have a high permeability and extended retention effect, making them an effective carrier material for drug delivery [19]. Ring polymers are formed by the operation of joining the free ends of a linear polymer chain together. As a result, linear chains are frequently found in ring polymers [24,25]. Even a small amount of the linear polymer can greatly slow down the ring-linear blends' overall kinetics. The conformational and dynamic behavior of ring chains in linear chains has recently become a focus of investigation.

According to Kapnistos et al., cyclic polystyrene ring contamination of less than 1% of linear chains (160 kDa) is sufficient to drastically reduce the linear viscoelastic response [26]. Gooßen et al. employed neutron spin echo spectroscopy to investigate the tangling dynamics of chains in a linear chain matrix using a relatively small number of ring chains as probes. They discovered that the host entirely controls the segmental dynamics of polymer rings immersed in linear chains [27]. In fact, there is the polymer interpenetration effect between ring chains and linear chains in polymer blends. This



Citation: Zhou, X.; Qin, Y. The Dynamic Behavior of a Single Semiflexible Ring Chain in a Linear Polymer Matrix. *Biophysica* **2023**, *3*, 476–484. <https://doi.org/10.3390/biophysica3030031>

Academic Editor: Attila Borics

Received: 26 June 2023

Revised: 13 July 2023

Accepted: 20 July 2023

Published: 26 July 2023



Copyright: © 2023 by the authors. Licensee MDPI, Basel, Switzerland. This article is an open access article distributed under the terms and conditions of the Creative Commons Attribution (CC BY) license (<https://creativecommons.org/licenses/by/4.0/>).

has been widely observed by experiments [28,29] and theoretical simulations [30]. Using single-molecule methods, Zhou et al. studied the dynamics of DNA rings in mixtures of ring-linear polymers. They discovered a large conformational fluctuation for rings in a steady extensional flow, and further found linear chains threading through open rings [29]. Yang et al. studied the conformation and kinetic characteristics of the ring polymer in linear polymers using the Monte Carlo simulation method. The diffusion path of the ring chain is made up of distinct fragments, and they proposed various threading techniques for rings [30].

In this study, we build a system composed of a linear polymer matrix and a single semiflexible ring chain. By using molecular dynamic simulation, we investigate the microscopic physical mobility of the semiflexible ring chain. We focused on the distribution properties and dynamics of the semiflexible ring in blends. Because of the hollow and disc-shaped feature of the semiflexible ring, it has two distinct characteristic directions: parallel to the plane direction and the normal direction. Previous studies have emphasized the overall motion of flexible ring chains in blends, whereas we concentrated on comparing the movements of the semiflexible ring parallel to the plane direction and in the normal direction. We compute the relaxation time of the ring in the normal and orientation directions. The relaxation time in the normal direction increases significantly when the swing movement in the normal direction of the ring is significantly constrained as $K_{b-linear}$ increases. This is because linear chains tend to be rod-like with a parallel arrangement as their bending energy increases. Additionally, the hollow part of the ring chain is filled with bundles of rod-like semiflexible linear chains.

There are the following sections in this article: The model and simulation details are given in Section 2. Our findings regarding the dynamic performance of a single semiflexible ring chain in a linear polymer matrix are described in Section 3; the conclusion is offered in Section 4. The simulation results can help us to understand the microscopic physical mechanisms of the movement of the ring chain in ring-linear polymer blends.

2. Model and Method

We adopt the classical bead spring model, which is frequently used in polymer simulations [31–37] to simulate the polymer chain, for the whole simulation process. Each chain is composed of L spherical monomers with a diameter of σ and a mass of m . Additionally, the length of the ring is $L_{ring} = 30$, and the length of the linear chain is $L_{linear} = 30$. Each chain's potential energy is found by the following equation:

$$U = U_{bond} + U_{angle} + U_{LJ} \quad (1)$$

where adjacent monomers of the chain are connected to each other by finite stretchable nonlinear elasticity (FENE) potentials:

$$U_{bond}(r) = -\frac{KR_0^2}{2} \ln\left[1 - \left(\frac{r - r_0}{R_0}\right)^2\right], r_0 < R_0 \quad (2)$$

where r_0 is the distance between two adjacent monomers of a polymer chain. $K = 30 k_B T / \sigma^2$ is the spring coefficient, and the finite ductility correlation parameter $R_0 = 1.5\sigma$ is used to avoid chain crossing.

We introduce the bond angle potential energy between neighboring bonds, which is widely used in polymer simulations [31,32], to describe the rigid feature of the semiflexible chains:

$$U_{angle} = K_{bending}[1 - \cos(\theta - \theta_0)] \quad (3)$$

where θ is the angle between two adjacent bonds, and $K_{bending}$ is the bending energy. The unit of $K_{bending}$ is $k_B T$, and all simulations are carried out at $k_B T = 1.0$ in our system. K_{b-ring} represents the bending energy of the ring chain, while $K_{b-linear}$ represents the bending energy of the linear chain. Additionally, θ_0 is the equilibrium value of the angle. For rings,

$\theta_0 = [\pi \times (L_{\text{ring}} - 2)]/L_{\text{ring}}$, $\theta_0 = [\pi \times (30 - 2)]/30 = 0.93\pi$. In the coarse-grained model developed in this study, $\theta_0 = \pi$ for linear chains. When K_{bending} is larger, the chain is more difficult to bend, that is, the chain is rigid. In this paper, the bending energy of the ring is fixed as $K_{\text{b-ring}} = 50$, and the bending energy of the linear chain ranges from $K_{\text{b-linear}} = 0$ to $K_{\text{b-linear}} = 50$.

To prevent overlap between all monomers of chains, all bonded and non-bonded monomer interactions use the modified Lennard-Jones potential:

$$U_{\text{LJ}}(r) = \begin{cases} 4\epsilon \left[\left(\frac{\sigma}{r}\right)^{12} - \left(\frac{\sigma}{r}\right)^6 + \frac{1}{4} \right], & r \leq 2^{1/6}\sigma \\ 0, & r > 2^{1/6}\sigma \end{cases} \quad (4)$$

where r is the distance between two monomers, and r_c is the truncation radius $r_c = 2^{1/6}\sigma$. It reaches zero at the minimum distance $r = r_c = 2^{1/6}\sigma$ of the respective Lennard-Jones potential, and is set to zero after that distance. That is, ring–ring, linear–linear, and ring–linear interactions are all pure repulsive forces, and $\epsilon = 1.0 \text{ k}_B\text{T}$ is the interaction strength.

The total particle number density of the ring–linear blends is defined by $\rho = (L_{\text{ring}} \times N_{\text{ring}} + L_{\text{linear}} \times N_{\text{linear}})/L^3 = 0.5$, where N_{ring} and N_{linear} are the number of ring chains and the number of linear chains, respectively, and L_{ring} and L_{linear} are the length of the ring chain and the length of the linear chain. In this study, $L_{\text{ring}} = 30$, $N_{\text{ring}} = 1$. The simulation parameters covered in this paper are given in Table 1. As the rigidity of the linear chain increases, it becomes more difficult for the system to be pressed to the target size. In order to ensure that the density of the system is about $\rho = 0.5$, the side length is around $L \approx 50$ for different $K_{\text{b-linear}}$. The stronger the rigidity, the greater the pressure required. For example, for $K_{\text{b-linear}} = 0$, the pressure is 0.381, and for $K_{\text{b-linear}} = 50$, the pressure is 0.451. Additionally, L_x , L_y , and L_z for all the systems is provided in Table 1. For our system, the pressure in the three directions is the same, all three directions are scaled in the same proportions, and the final target side length is the same: $L_x = L_y = L_z$.

Table 1. The detailed simulation parameters covered in this paper.

| L_{ring} | N_{ring} | L_{linear} | N_{linear} | $K_{\text{b-ring}}$ | $K_{\text{b-linear}}$ | Pressure | Side Length of Simulation Box $L_x/L_y/L_z$ | r_c |
|-------------------|-------------------|---------------------|---------------------|---------------------|-----------------------|----------|--|-----------|
| 30 | 1 | 30 | 2082 | 50 | 0 | 0.381 | 50.23 | $2^{1/6}$ |
| | | | | | 10 | 0.418 | 51.57 | |
| | | | | | 20 | 0.426 | 50.82 | |
| | | | | | 30 | 0.435 | 51.43 | |
| | | | | | 40 | 0.441 | 50.56 | |
| | | | | | 50 | 0.451 | 50.90 | |

At the initial moment, the ring and linear chains are first distributed at random in a very large simulation box. To achieve the necessary equilibrium density, the NPT series is employed as a thorough compression mechanism. In this process, different NPT parameters are used to compress the systems with different linear chain bending energies, as shown in column (8) of Table 1. The system is then balanced in the NVT ensemble, with a total running duration of 5×10^7 steps, where the first 10^7 steps are used to ensure balance. After Δt_1 , data are collected at intervals of 10^4 steps. We use a Nosé–Hoover thermostat; the reduced temperature is $T^* = 1.0$ in ϵ/k_B , the initial temperature $T_{\text{start}} = 1.0$, the end temperature $T_{\text{stop}} = 1.0$, the damping factor $T_{\text{damp}} = 0.5$, and the thermostat mass $m = 1.0$. The velocity Verlet algorithm is used to integrate Newtonian equations of motion with a time step of $\Delta t = 0.005\tau_0$, where $\tau_0 = (m\sigma^2/k_B T)^{1/2}$ is the inherent MD unit of time. The units of reduction $\sigma = 1$, $m = 1$, and $\tau_0 = (m\sigma^2/k_B T)^{1/2} = 1$ are the units of length, mass, and time, respectively. All simulations were carried out using the free and open-source

LAMMPS molecular dynamics software package (Sandia National Lab, Albuquerque, NM, USA) [38].

3. Result and Discussion

Figure 1 shows a schematic diagram of a semiflexible ring chain in a linear chain matrix with different bending energies. The linear chains are flexible, with $K_{b\text{-linear}} = 0$ in Figure 1a. As shown in Figure 1, the semiflexible ring chain presents a hollow two-dimensional flat disc shape, when the linear chain is flexible, linear chains are a spherical shape, and several linear chains are distributed in the middle of the circular chain, as shown in Figure 1a. As the bending energy of the linear chain increases, as shown in Figure 1b, the linear chain stretches and has a certain length with a radius of gyration $R_{g\text{-linear}} = 5.60$ for $K_{b\text{-linear}} = 10$, distributed around the ring chain. The bending energy is moderate for $K_{b\text{-linear}} = 10$, and linear chains are between a spherical shape and rod shape. As a result, the linear chains are bent and distributed across the hollow part of the ring chain, as shown in Figure 1b for a typical linear chain with $K_{b\text{-linear}} = 10$ highlighted in yellow. In both above cases, the diffusion in all directions of the ring chain is almost the same. As the bending energy of the linear chain increases to $K_{b\text{-linear}} = 50$, as shown in Figure 1c, the linear chain tends to be arranged in parallel, and penetrates the ring. This is mainly caused by the fact that there are ordered nematic phases in a semiflexible linear chain system at high monomer concentrations. All linear chains in our simulation are made up of 30 monomers, as the size of the linear chains depends on the chain stiffness; the root-mean square radius of gyration $R_{g\text{-linear}}$ ranges from 2.98 to 7.02 for linear chains when the bending energy of the chains increases from $K_{b\text{-linear}} = 0$ to 50, and $R_{g\text{-linear}} = 5.60$ for $K_{b\text{-linear}} = 10$ (see Figure S1 in the Supplementary Information). The hollow part of the ring chain is filled by bundles of rod-like semiflexible linear chains. For this condition, the diffusion of the ring chain parallel to the plane is limited, and the diffusion slows down significantly.

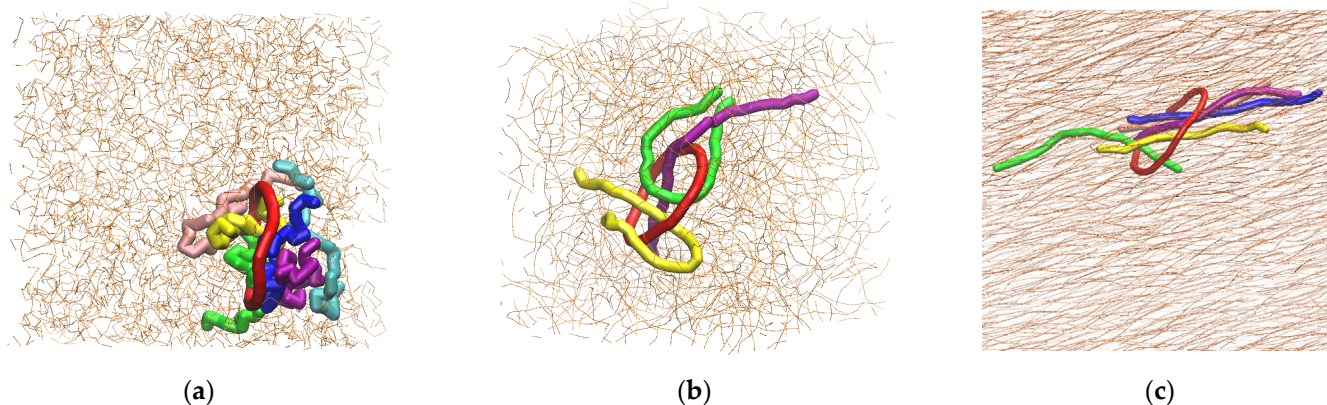


Figure 1. Snapshots of a single semiflexible ring chain in a linear polymer matrix with different bending energies: $K_{b\text{-linear}} = 0$ (a), $K_{b\text{-linear}} = 10$ (b), $K_{b\text{-linear}} = 50$ (c).

To discuss the relationship between the diffusion of the semiflexible ring chain and the rigidity of the linear chain, we calculate the non-Gaussian parameter Γ , defined as

$$\Gamma = \frac{3 \langle r^4(t) \rangle}{5 \langle r^2(t) \rangle^2} - 1 \quad (5)$$

where $r(t)$ is the displacement of the monomer of the ring chain from $t = 0$ to time t . If the ring chain is an ineffectual free-diffusion Brownian motion, correspondingly, $\Gamma = 0$ and the deviation of this parameter from $\Gamma = 0$ is a measure of the degree of the non-Gaussian function, as shown in the black line in Figure 2. As shown in Figure 2, the semiflexible ring has a non-Gaussian parameter Γ , close to zero in a flexible linear chain matrix, but for $K_{b\text{-linear}} = 50$, the motion of the semiflexible ring is hindered for a period of time. As shown

in Figure 1c, the linear chains pass through the center of the ring, the ring is trapped, and the movement slows down. The ring chain becomes subdiffused, and Γ has a distinct peak, as shown in the red line in Figure 2, which indicates the presence of kinetic heterogeneity. In fact, the diffusion of single particles in crystalline, glass, and granular fluids also satisfies non-Gaussian dynamics due to the escape “cage” process.

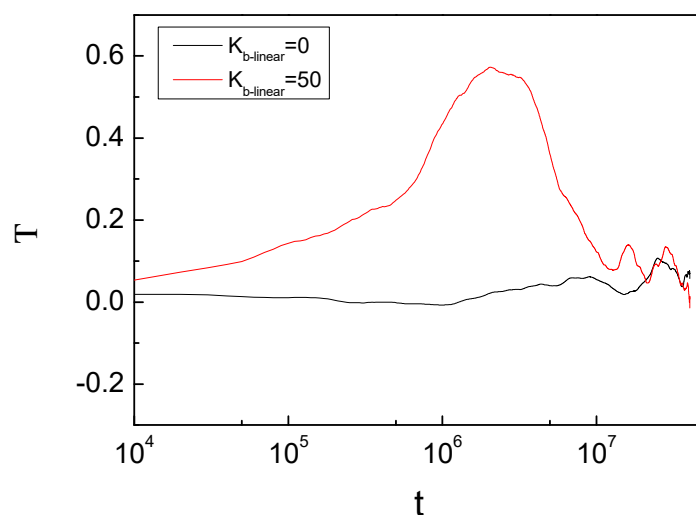


Figure 2. Non-Gaussian parameters Γ of the semiflexible ring chain in linear chains with different bending energies $K_{b\text{-linear}}$.

The relative orientations of linear chains can also be measured quantitatively as follows:

$$S = \langle (3\cos^2\theta - 1)/2 \rangle \quad (6)$$

where θ is the angle of two neighboring linear chains. The average orientation S will take values of 0 and 1 for one linear chain randomly oriented and parallel to another. For flexible linear polymers ($K_{b\text{-linear}} = 0$), the value of S remains nearly constant at 0, and linear chains are always oriented randomly. However, for rod-like linear polymers with $K_{b\text{-linear}} = 50$, Figure 3 shows that S has a maximum of 0.74, indicating that they are almost parallel with respect to each other for linear chains.

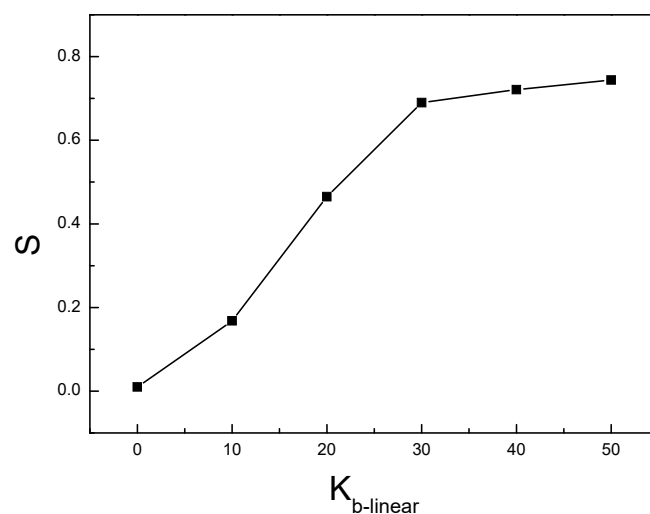


Figure 3. Average orientation order parameter S of linear polymers as function of $K_{b\text{-linear}}$.

Dynamic heterogeneity is more directly expressed as diffusion trajectories. If the ring is not passed through the center by a linear chain and is briefly caged, the diffusion will

be relatively fast, and will behave like a random walk. However, if the ring is crossed by a rod-like linear chain, the diffusion becomes slow. Figure 4 shows the typical diffusion trajectories of a typical ring chain in different rigid linear chain matrices.

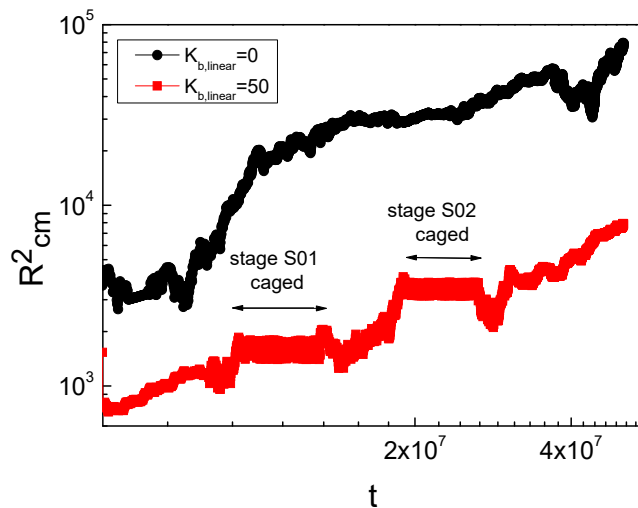


Figure 4. Representative trajectories of a semiflexible ring chain in a linear chain with different bending energies $K_{b-linear}$.

R_{cm}^2 in Figure 4 represents the “diffusion trajectory” of the semiflexible ring chain, i.e., the square displacement of the centroid of the ring from the corresponding simulated sample at a certain moment relative to the initial position and zero time. For the ring diffused in the flexible linear chain matrix, such as the black curve in Figure 4, random walk diffusion behavior can always be found. However, for the semiflexible linear chain system of Figure $K_{b-linear} = 50$, the red curve shows a shorter plateau, as shown in Figure 4, a plain that is temporarily stuck due to the ring being bound by the linear chain through for stage S01. After this chain is temporarily removed at S01, linear chains can be retracted or “slipped” from the ring relatively easily. From the corresponding molecular conformation, it is found that the rings are still connected along the trajectory segment between stage S01 and stage S02. The ring is soon crossed by another chain, corresponding to stage S02, as shown in the illustration. The plateau becomes more visible in the figure. After stage S02, the chain temporarily escapes the caged state, and the ring begins to return to normal diffusion.

For a ring oriented and threaded by linear chains, we compare the diffusional relaxation time with the auto-correlation time of the normal vector (the direction of the black arrow in the illustration of Figure 5) and the orientation vector of the chains (the direction of the red arrow in the illustration of Figure 5) of the ring.

We compute the auto-correlation function of the normal vector of rings, $\rho_u(t)$, defined by

$$\rho_u(t) = \frac{\vec{u}(t) \bullet \vec{u}(0)}{\langle u^2 \rangle} \tag{7}$$

where the normal vector $\vec{u}(t)$ is calculated by $\vec{u}(t) = \sum_i \vec{b}_i \times \vec{b}_{i+1}$, with b_i as the corresponding bond vector. The relaxation time, τ_{normal} , was estimated by fitting an unweighted least squares line to the linear, long-time region of a semilog plot of $\rho_u(t)$ vs. time (see Figure 5). The inverse of the relaxation time is the negative of the slope of the line.

The auto-correlation function of the orientation vector of rings, $\rho_{R'}(t)$, is defined by

$$\rho_{R'}(t) = \frac{\vec{R}'(t) \bullet \vec{R}'(0)}{\langle R'^2 \rangle} \tag{8}$$

where the orientation vector, $\vec{R}'(t)$ is defined as $\vec{R}'(t) = \sum_{i=0}^{N_{ring}/2} \vec{b}_i$, with b_i as the corresponding bond vector. The relaxation time, $\tau_{orientation}$, was estimated by fitting an unweighted least squares line to the linear, long-time region of a semilog plot of $\rho_{R'}(t)$ vs. time (see Figure 5). The inverse of the relaxation time is the negative of the slope of the line. As $K_{b-linear}$ increases, the ring chain is threaded by linear chains, the central part of the semiflexible ring is filled, the left and right swing movement in the normal direction is significantly limited, and the relaxation time in the normal direction increases significantly, from $\tau_{normal} = 113,378$ for $K_{b-linear} = 0$ to $\tau_{normal} = 590,000$ for $K_{b-linear} = 50$, as shown in Table 2. The diffusion is dominated by the motion along the orientation direction of the ring. Our simulation time for balancing is significantly longer than the slowest of the four relaxation times.

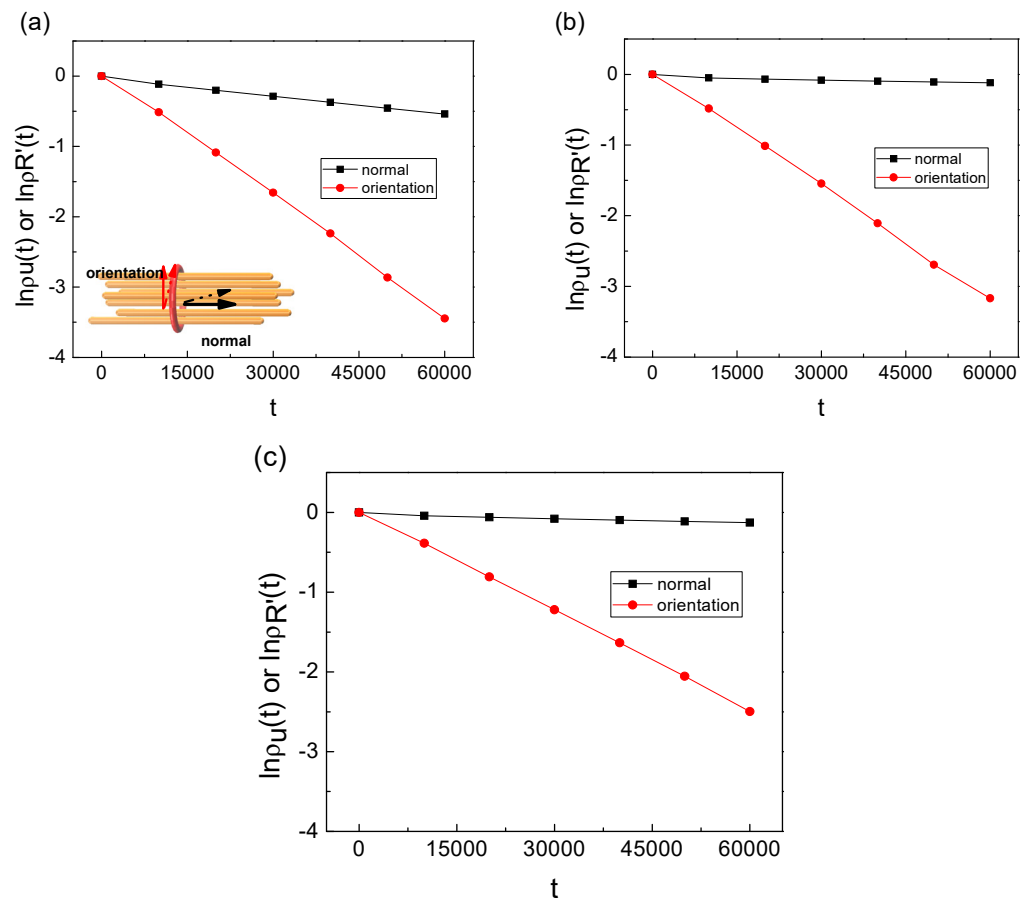


Figure 5. $\ln \rho_n(t)$ or $\ln \rho_{R'}(t)$ as a function of t for a semiflexible ring chain for $K_{b-linear} = 0$ (a), $K_{b-linear} = 10$ (b), $K_{b-linear} = 50$ (c).

In fact, due to the formation of a ring-threaded phenomenon in the semiflexible linear chain, the diffusion of the ring chain in the blend system is slow. As shown in the table below, as $K_{b-linear}$ increases, the gap between τ_{normal} and $\tau_{orientation}$ gradually becomes larger, which is consistent with the screenshot shown in Figure 1c. Additionally, the normal relaxation time of the semiflexible ring is much longer than the relaxation time of the parallel direction $\tau_{normal} > \tau_{orientation}$, that is, the semiflexible ring spreads along the extension direction of the rod-like linear chain through its center. However, it is temporarily confined to the cage in the direction of the plane parallel. Our results help us to understand the special topological conformation and dynamic behavior of the semiflexible ring in ring-linear polymer blend systems.

Table 2. The relaxation times τ_{normal} and $\tau_{\text{orientation}}$ for a semiflexible ring chain in linear chains with different bending energies $K_{\text{b-linear}}$.

| $K_{\text{b-linear}}$ | $\tau_{\text{orientation}}$ | τ_{normal} |
|-----------------------|-----------------------------|------------------------|
| 0 | 17,295 | 113,378 |
| 10 | 18,642 | 561,797 |
| 20 | 20,000 | 572,100 |
| 30 | 22,000 | 579,100 |
| 40 | 23,000 | 582,400 |
| 50 | 24,026 | 590,000 |

4. Conclusions

The dynamic behavior of ring chains in ring-linear polymer blends has long been a study focus in polymer simulation. Based on the coarse-grained model, the molecular dynamics method is employed in this research to investigate the dynamic behavior of a single ring chain in a linear chain matrix. The semiflexible ring chain is stretched out into a cannulated circular shape with hollow construction, and the linear chain occupies the middle part. As the linear chain's bending energy increases, the linear chains tend to be organized parallel to one another and pass through the circular chain. The swing of the ring chain in its normal direction is limited for a larger $K_{\text{b-linear}}$ value, and the relaxation time in the normal direction grows dramatically. Our research can be used to better comprehend the microphysical motion processes of semiflexible ring chains in linear polymers.

Supplementary Materials: The following supporting information can be downloaded at: <https://www.mdpi.com/article/10.3390/biophysica3030031/s1>, Figure S1. The root-mean-square radius of gyration of linear chains $R_{\text{g-linear}}$ as a function of $K_{\text{b-linear}}$.

Author Contributions: Conceptualization, X.Z.; methodology, X.Z.; resources, X.Z.; data curation, X.Z.; supervision, X.Z.; funding acquisition, X.Z.; writing, original draft preparation, X.Z.; writing, review and editing, X.Z. and Y.Q. All authors have read and agreed to the published version of the manuscript.

Funding: This work was supported by the Fundamental Research Funds for the Central Universities (grant no. 3072021CFT2508), the National Defense Basic Research Program of China (grant no. JCKYS2023604SSJS003), and the Fundamental Research Funds of Harbin Engineering University (grant no. 3072023CFJ2501).

Data Availability Statement: The data that support the findings of this study are available from the corresponding author, [Xiaolin Zhou], upon reasonable request.

Conflicts of Interest: The authors declare no conflict of interest.

References

1. Craig, I.R.; Manolopoulos, D.E. Quantum statistics and classical mechanics: Real time correlation functions from ring polymer molecular dynamics. *J. Chem. Phys.* **2004**, *121*, 3368–3373. [[CrossRef](#)]
2. Pioper, P.; Likos, C.N.; Moreno, A.J.; Blaak, R. An anisotropic effective model for the simulation of semiflexible ring polymers. *Macromolecules* **2015**, *48*, 4983.
3. Narros, A.; Likos, C.N.; Moreno, A.J.; Capone, B. Multi-blob coarse graining for ring polymer solutions. *Soft Matter* **2014**, *10*, 9601. [[CrossRef](#)]
4. Slimani, M.Z.; Bacova, P.; Bernabei, M.; Narros, A.; Likos, C.N. Cluster glasses of semiflexible ring polymers. *ACS Macro. Lett.* **2014**, *3*, d611. [[CrossRef](#)] [[PubMed](#)]
5. Narros, A.; Moreno, A.J.; Likos, C.N. Effects of knots on ring polymers in solvents of varying quality. *Macromolecules* **2013**, *46*, 3654. [[CrossRef](#)]
6. Richardson, J.O.; Althorpe, S.C. Ring-polymer molecular dynamics rate-theory in the deep-tunneling regime: Connection with semiclassical instanton theory. *J. Chem. Phys.* **2009**, *131*, 214106. [[CrossRef](#)] [[PubMed](#)]
7. Halverson, J.D.; Lee, W.B.; Grest, G.S.; Grosberg, A.Y.; Kremer, K. Molecular dynamics simulation study of nonconcatenated ring polymers in a melt. II. Dynamics. *J. Chem. Phys.* **2011**, *134*, 204905. [[CrossRef](#)] [[PubMed](#)]

8. Michieletto, D.; Turner, M.S. A topologically driven glass in ring polymers. *Proc. Natl. Acad. Sci. USA* **2016**, *113*, 5195. [[CrossRef](#)]
9. Obukhov, S.P.; Rubinstein, M.; Duke, T. Dynamics of a ring polymer in a gel. *Phys. Rev. Lett.* **1994**, *73*, 1263–1266. [[CrossRef](#)]
10. Reigh, S.Y.; Yoon, D.Y. Single-molecule Imaging reveals topology dependent mutual relaxation of polymer chains. *ACS Macro Lett.* **2013**, *2*, 296. [[CrossRef](#)]
11. Trabi, M.; Craik, D.J. Circular proteins: No end in sight. *Trends Biochem. Sci.* **2002**, *27*, 132–138. [[CrossRef](#)]
12. Dobay, A.; Dubochet, J.; Millett, K.; Stasiak, A. Scaling behavior of random knots. *Proc. Natl. Acad. Sci. USA* **2003**, *100*, 5611–5615. [[CrossRef](#)] [[PubMed](#)]
13. Sanchez, T.; Kulic, I.M.; Dogic, Z. Circularization, photomechanical switching, and a supercoiling transition of actin filaments. *Phys. Rev. Lett.* **2010**, *104*, 4. [[CrossRef](#)] [[PubMed](#)]
14. Greene, J.; Baird, A.M.; Brady, L.; Lim, M.; Gray, S.G.; McDermott, R.; Finn, S.P. Circular RNAs: Biogenesis, Function and Role in Human Diseases. *Front. Mol. Biosci.* **2017**, *4*, 11. [[CrossRef](#)] [[PubMed](#)]
15. Lasda, E.; Parker, R. Circular RNAs: Diversity of form and function. *RNA* **2014**, *20*, 1829–1842. [[CrossRef](#)]
16. Liang, X.G.; Chen, H.; Li, L.; An, R.; Komiyama, M. Ring-Structured DNA and RNA as Key Players In Vivo and In Vitro. *Bull. Chem. Soc. Jpn.* **2021**, *94*, 141–157. [[CrossRef](#)]
17. Deutsch, J.M. Equilibrium size of large ring molecules. *Phys. Rev. E* **1999**, *59*, R2539–R2541. [[CrossRef](#)]
18. Meaburn, K.J.; Misteli, T. Cell biology—Chromosome territories. *Nature* **2007**, *445*, 379–381. [[CrossRef](#)]
19. Fariyah, M.H.; Scott, M.G. The synthesis, properties and potential applications of cyclic polymers. *Nat. Chem.* **2020**, *12*, 433–444.
20. Jacob, F.; Wollman, E.L. Les épisomes, éléments génétiques ajoutés. *Seances Acad. Sci.* **1958**, *247*, 154.
21. Nasongkla, N.; Chen, B.; Macaraeg, N.; Fox, E.; Fréchet, J.M.J.; Szoka, F.C. Dependence of pharmacokinetics and biodistribution on polymer architecture: Effect of cyclic versus linear polymers. *J. Am. Chem. Soc.* **2009**, *131*, 3842. [[CrossRef](#)] [[PubMed](#)]
22. Poelma, J.E.; Ono, K.; Miyajima, D.; Aida, T.; Satoh, K.; Hawker, C.J. Cyclic block copolymers for controlling feature sizes in block copolymer lithography. *ACS Nano* **2012**, *6*, 10845. [[CrossRef](#)] [[PubMed](#)]
23. Bennour, H.; Fildier, A.; Chatti, S.; Kricheldorf, H.R.; Zina, M.S.; Medimagh, R. Biosourced cyclic and multicyclic polyesters based on 1, 4: 3, 6-dianhydrohexitols: Application to metal ions uptake in aqueous media. *Macromol. Chem. Phys.* **2015**, *216*, 1081. [[CrossRef](#)]
24. Roovers, J.; Toporowski, P.M. Synthesis of high molecular weight ring polystyrenes. *Macromolecules* **1983**, *16*, 843–849. [[CrossRef](#)]
25. McKenna, G.B.; Hadziioannou, G.; Lutz, P.; Hild, G.; Strazielle, C.; Straupe, C.; Rempp, P. Dilute solution characterization of cyclic polystyrene. *Macromolecules* **1987**, *20*, 498–512. [[CrossRef](#)]
26. Kapnistos, M.; Lang, M.; Vlassopoulos, D.; Pyckhout-Hintzen, W.; Richter, D.; Cho, D.; Chang, T.; Rubinstein, M. Unexpected power-law stress relaxation of entangled ring polymers. *Nat. Mater.* **2008**, *7*, 997–1002. [[CrossRef](#)]
27. Gooßen, S.; Krutyeva, M.; Sharp, M.; Feoktystov, A.; Allgaier, J.; Pyckhout-Hintzen, W.; Wischnewsiki, A.; Richter, D. Sensing polymer chain dynamics through ring topology: A neutron spin echo study. *Phys. Rev. Lett.* **2015**, *115*, 148302.
28. Wang, Z.W.; Mei, L.; Guo, C.X.; Huang, S.; Shi, W.Q.; Li, X.W.; Feng, W.; Li, X.P.; Yang, C.; Yuan, L.H. Supramolecular shish kebabs: Higher order dimeric structures from ring-in-rings complexes with conformational adaptivity. *Angew. Chem. Int. Ed.* **2023**, *62*, e202216690. [[CrossRef](#)]
29. Zhou, Y.C.; Young, C.D.; Lee, M.; Banik, S.; Kong, D.; McKenna, G.B.; Robertson-Anderson, R.M.; Sing, C.E.; Schroeder, C.M. Dynamics and rheology of ring-linear blend semidilute solutions in extensional flow: Single molecule experiments. *J. Rheol.* **2021**, *65*, 729–744. [[CrossRef](#)]
30. Yang, Y.B.; Sun, Z.Y.; Fu, C.L.; An, L.J.; Wang, Z.G. Monte Carlo simulation of a single ring among linear chains: Structural and dynamic heterogeneity. *J. Chem. Phys.* **2010**, *133*, 064901. [[CrossRef](#)]
31. Bernabei, M.; Bacova, P.; Moreno, A.J.; Narros, A.; Likos, C.N. Fluids of semiflexible ring polymers: Effective potentials and clustering. *Soft Matter* **2013**, *9*, 1287–1300. [[CrossRef](#)]
32. Poier, P.; Bačová, P.; Moreno, A.J.; Likos, C.N.; Blaak, R. Anisotropic effective interactions and stack formation in mixtures of semiflexible ring polymers. *Soft Matter* **2016**, *12*, 4805–4820. [[CrossRef](#)] [[PubMed](#)]
33. Halverson, J.D.; Lee, W.B.; Grest, G.S.; Grosberg, A.Y.; Kremer, K. Molecular dynamics simulation study of nonconcatenated ring polymers in a melt. I. Statics. *J. Chem. Phys.* **2011**, *134*, 204904. [[CrossRef](#)]
34. Lee, E.; Jung, Y.J. Segregated structures of ring polymer melts near the surface: A molecular dynamics simulation study. *Soft Matter* **2015**, *11*, 6018–6028. [[CrossRef](#)]
35. Smith, J.S.; Bedrov, D.; Smith, G.D.; Compos, G.D. A molecular dynamics simulation study of nanoparticle interactions in a model polymer-nanoparticle composite. *Composites Sci. Technol.* **2003**, *63*, 1599. [[CrossRef](#)]
36. Liu, J.; Cao, D.; Zhang, L. Molecular dynamics study on nanoparticle diffusion in polymer melts: A test of the Stokes-Einstein Law. *J. Phys. Chem. C* **2008**, *112*, 6653. [[CrossRef](#)]
37. Weeks, J.D.D.; Andersen, H.C. Role of repulsive forces in determining the equilibrium structure of simple liquids. *J. Chem. Phys.* **1971**, *54*, 5237. [[CrossRef](#)]
38. Plimpton, S. Fast parallel algorithms for short-range molecular dynamics. *J. Comput. Phys.* **1995**, *117*, 1–19. [[CrossRef](#)]

Disclaimer/Publisher’s Note: The statements, opinions and data contained in all publications are solely those of the individual author(s) and contributor(s) and not of MDPI and/or the editor(s). MDPI and/or the editor(s) disclaim responsibility for any injury to people or property resulting from any ideas, methods, instructions or products referred to in the content.